RSC Advances

This is an *Accepted Manuscript*, which has been through the Royal Society of Chemistry peer review process and has been accepted for publication.

Accepted Manuscripts are published online shortly after acceptance, before technical editing, formatting and proof reading. Using this free service, authors can make their results available to the community, in citable form, before we publish the edited article. This *Accepted Manuscript* will be replaced by the edited, formatted and paginated article as soon as this is available.

You can find more information about *Accepted Manuscripts* in the Information for Authors.

Please note that technical editing may introduce minor changes to the text and/or graphics, which may alter content. The journal's standard Terms & Conditions and the Ethical guidelines still apply. In no event shall the Royal Society of Chemistry be held responsible for any errors or omissions in this *Accepted Manuscript* or any consequences arising from the use of any information it contains.

ROYAL SOCIETY OF CHEMISTRY

www.rsc.org/advances

Please do not adjust margins

Journal Name

ARTICLE

Poly(vinyl alcohol)/graphene oxide nanocomposites prepared by in situ polymerization with enhanced mechanical properties and water vapor barrier properties

Received 00th January 20xx,
Accepted 00th January 20xx

DOI: 10.1039/x0xx00000x

www.rsc.org/

Jiaojiao Ma,[ab] Ying Li,[a] Xiande Yin,[a] Yu Xu,[a] Jia Yue[a], Jianjun Bao*[ab] and Tao zhou*[a]

This paper described a novel and bottom-up in situ polymerization method for preparing the poly(vinyl alcohol) (PVA)/graphene oxide (GO) nanocomposites. The approach is conducted by mixing the vinyl acetate, methanol, initiator and GO at the aid of high power ultrasonic, followed by free radical polymerization and alcoholysis reaction, resulting in the in situ formation of PVA matrix and molecular level dispersion of GO. X-ray diffraction, transmission electron microscopy and scanning electron microscopy revealed that GO nanosheets were completely intercalated, uniformly dispersed and highly oriented along the surface of nanocomposite films. Centrifugation experiments, fourier-transform infrared spectroscopy and differential scanning calorimetry evidenced the existence of strong hydrogen bond interactions between the GO nanosheets and PVA matrix. Furthermore, the mechanical properties and water vapor barrier properties of PVA/GO nanocomposites had been strikingly enhanced by adding a small content of GO (with GO loading as low as 0.01-0.08 wt%). Compared with the neat polymer, the tensile strength increased from 42.3 to 50.8 MPa and Young's modulus increases markedly from 1477 to 2123 MPa at the GO incorporation of only 0.04 wt%. Moreover, it gave rise to about 78% decline in the coefficient of moisture permeability.

1. Introduction

Currently, polymer materials with good gas barrier properties and enhanced mechanical properties are in great demand in the applications of packaging industry, electronics, and fuel cell industry.[1-5] Poly(vinyl alcohol) (PVA), due to its excellent film forming and oxygen barrier properties as well as water-soluble and non-toxic properties, has been widely used in the packaging and protective coating.[6-9] However, the abundant hydroxyl groups of PVA make it extremely easy to be plasticized by water, which results in the poor water vapor barrier properties.[10] Besides, the effect of swelling and plasticizing would cause a great decline in mechanical properties, which extremely limits its application.[11,12] Fortunately, graphene or graphene oxide (GO), with its super-mechanical properties, high specific area (2600 m^2/g), and excellent impermeability to all gas molecules,[13-17] have been demonstrated as efficient nanofillers to improve both the mechanical properties and the water vapor barrier properties.[18,19]

A variety of routes[20-22] have been developed to fabricate PVA/GO composites, among which the most common method is solution mixing.[23,24] However, it is well-known that GO sheets have a collective behaviour to form GO papers, which are "paperlike" composites composed of stacked GO sheets in solution. The collective behaviour results in poor interaction between the fillers and polymer matrices and limits the dispersion of GO, which largely decreases the reinforcing efficiency. So numbers of attempts such as chemical modification of GO have been made to improve the solubility and dispersion of GO sheets in polymer systems.[25,26] Nonetheless, this method always needs activator or catalyst, tough experimental conditions as well as complicated operation processes. Layer-by-layer (LBL) self-assembly[27] is considered as another effective method to prepare polymer/GO nanocomposites. However, the method is limited by the complex operation processes, repeated deposition cycles and time-consuming purification steps. Therefore, it is still necessary to explore a more convenient and efficient approach to prepare PVA/GO composites with uniform dispersion state of GO sheets on the molecular scale in the polymer matrix.

Therefore, in situ polymerization, showing a high level of dispersion of nanofiller, has been proved to be an effective and facile approach to fabricate polymer/GO composites.[28,29] Huang et al.[30] prepared PP/GO nanocomposites via in situ intercalative polymerization using Ziegler-Natta catalyst. The GO nanosheets are well exfoliated and homogenously dispersed in the PP matrix. Zhen Xu and Chao Gao[31] reported that they had prepared nylon-6-graphene composites by in

[a] State Key Laboratory of Polymer Materials Engineering of China, Polymer Research Institute, Sichuan University, Chengdu 610065, China. E-mail: jjbao2000@sina.com; zhoutaopoly@scu.edu.cn; Fax: +86-28-85402465; Tel: +86-28-85402601
[b] Research Center for Application of Graphene, (Sichuan University-WuXi), Wuxi, 214000, China

RSC Advances Accepted Manuscript

Please do not adjust margins

situ polymerization, the tensile strength and Young's modulus of which increased by 2.1 folds and 2.4 folds with the graphene loading of only 0.1 wt%. Because of structural analogy, the same methodology could be applied for synthesizing PVA/GO or PVA/graphene nanocomposites. But the PVA is always prepared from hydrolysis of poly(vinyl acetate) (PVAc),[32,33] so the key issue is successfully manufacturing the excellent dispersion of GO in hydrophobic PVAc matrix. Zheng et al.[34] prepared PVAc intercalated graphite oxide nanocomposites by in situ intercalative polymerization. As the raw material is non-exfoliated graphite oxide, the intercalation of monomer into graphite oxide is so difficult that the n-octanol/graphite oxide intercalated composites needs to be synthesized at first. But along with the growing expertise in fabricating the intercalation of graphite oxide into monolayer GO by physical or chemical methods, using exfoliated GO as raw material, the fabrication of homogeneous PVAc/GO nanocomposites has proved to be feasible and efficient at the help of ultrasonic stresses.[35-37]

Herein, in this article, we reported a new bottom-up and one-step in situ polymerization method for the preparation of PVA/GO nanocomposites. The whole process can be outlined in Fig. 1. The approach was carried out by the homogeneous mixing of vinyl acetate (VAc), methanol, azoisobutyronitrile (AIBN) and GO at the aid of high power ultrasonication treatment, followed by an in situ radical polymerization and alcoholysis reaction. The ultrasonic stresses contributed to improving the efficiency and capacity of producing a kind of sponge effect and facilitating the intercalation of small molecules into the interlayers of GO.[38,39] It should be noted the intercalated GO nanosheets were homogenously dispersed and highly oriented in composites and had strong hydrogen bonding interactions with PVA molecular chains. Moreover, these nanocomposites with trace amount of GO (only 0.01-0.08 wt%) showed significant enhancement in mechanical properties and gas barrier properties. Besides, this in situ polymerization can directly synthesize the PVA/GO nanocomposites without redissolving and drying process, which can greatly reduce the consumption of energy. This one-step process would also shorten the reaction time, simplify the operational process and lower the cost compared with the other methods. That is, the in situ method opened a novel strategy to produce PVA/GO or PVA/graphene nanocomposites. It not only realized the delamination and dispersion of GO, but also improved the mechanical properties and water vapor barrier properties of PVA by one step.

2. Experiment

2.1. Materials

Crystalline flake graphite was purchased from Qingdao Tianheda Graphite Co., Ltd (China). Vinyl acetate (VAc)

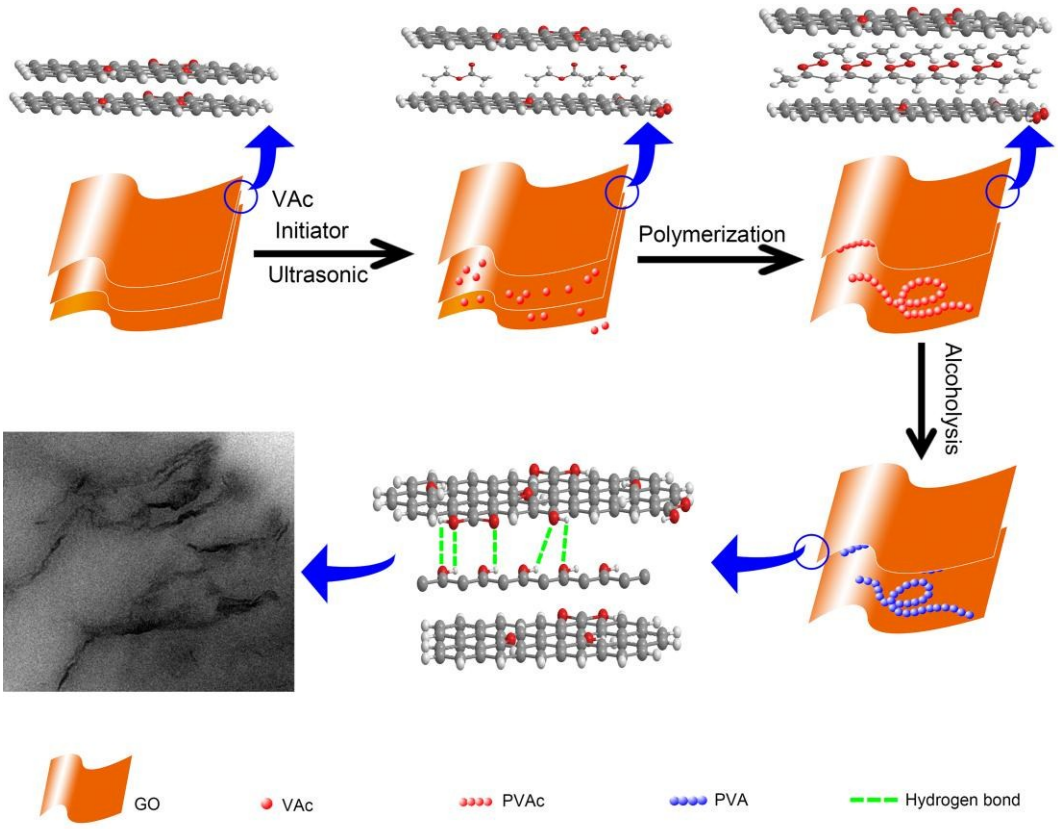

Fig. 1 Schematic illustration of the preparation of PVA/GO nanocomposites.

RSC Advances Accepted Manuscript

This journal is © The Royal Society of Chemistry 20xx

(Sichuan Vinylon Works, 99.0%) was distilled under reduced pressure to remove inhibitors. Azobisisobutyronitrile (AIBN) (Tianjing Kermel Chemical Reagents, 99.0%) was refined by recrystallization in methanol before use. Methanol was purchased from Chengdu Kelong Chemical Reagent Factory (China). Sodium hydroxide (NaOH, 99.9%) was obtained from Sinopharm Chemical Reagent Co., Ltd (China). The reagents were all of analytical grade. The water used in the whole experiment was deionized.

2.2. Synthesis of GO and PVA/GO nanocomposites by in situ polymerization

GO was prepared according to a modified Hummer's method.[40,41] Then the homogeneous and exfoliated GO suspension was put into freezer dryer for 3 days. Transmission electron microscopy (TEM), Scanning electron microscopy (SEM), Atomic force microscopy (AFM) and X-ray photoelectron spectroscopy (XPS) images of the synthesized GO are shown in Fig. 2.

The process of preparing PVA/GO nanocomposites by in situ polymerization is showed as follows:

(1) The preparation of PVAc/GO nanocomposites

The polymerization reaction was carried out in a 250 ml glass reactor equipped with a reflux condenser, a mechanical stirrer, and a nitrogen inlet. In a typical reaction system, 0.04 g of as-synthesized GO was diluted into 25 g of methanol and treated under ultrasonic (600 W) for 0.5 h. Then the mixture was added into the reactor. 100 g of VAc and 0.1 g of AIBN were added to the mixture, followed by ultrasonic treatment (600 W) for another 0.5 h and mechanical stirring for 3 h to make homogeneous solution. Then the system was refluxed at 65 °C for 4 h under nitrogen atmosphere. After polymerization,

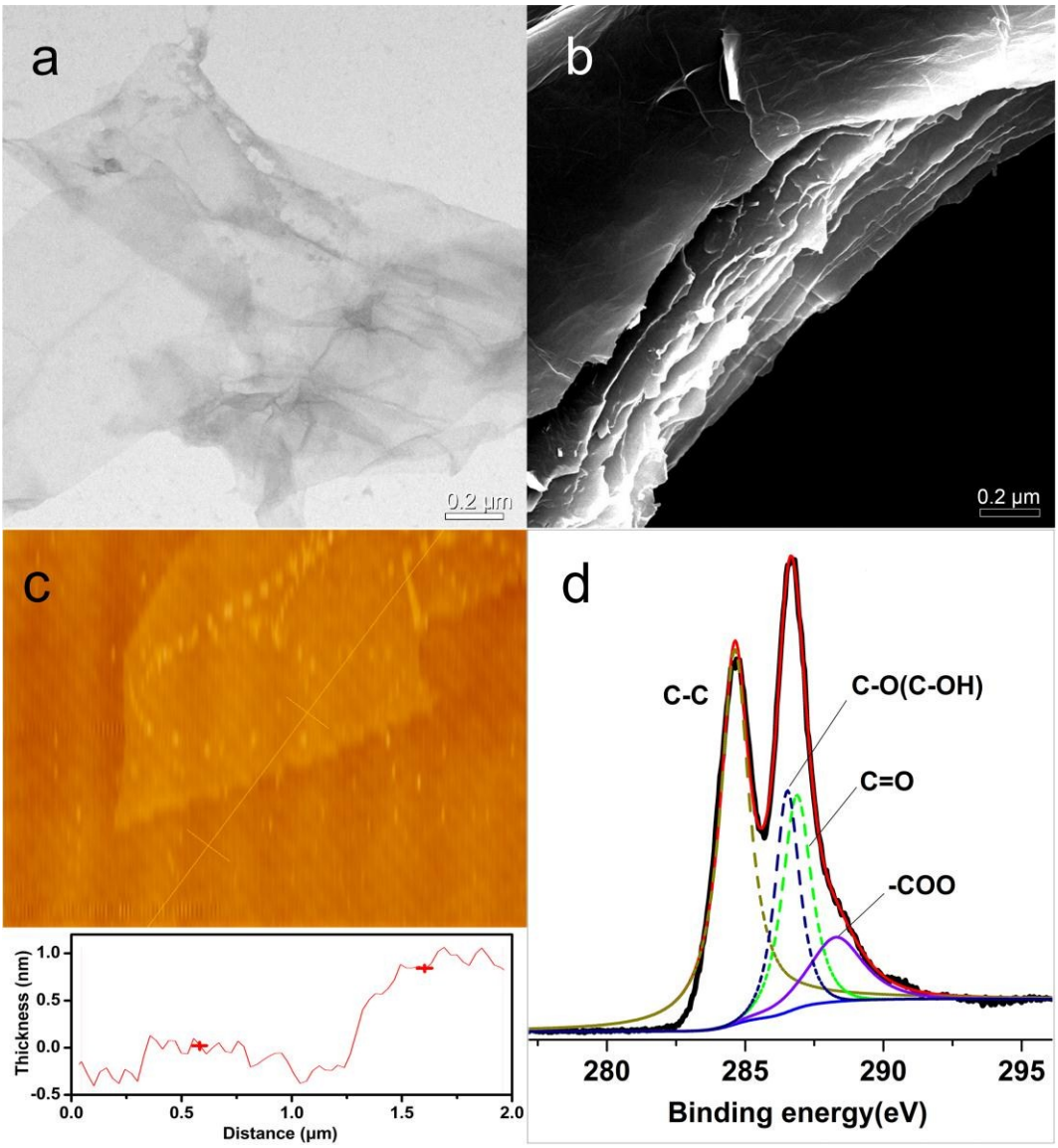

Fig. 2 Characterization of GO. (a) TEM image, (b) SEM image, (c) AFM image, and (d) XPS spectrum (C1s) of the GO nanosheets.

RSC Advances Accepted Manuscript

the product was distilled under reduced pressure three times to remove the residual monomers. At last the PVAc/GO nanocomposites were dried in vacuum oven at 50 °C for 24 h.

(2) The alcoholysis reaction

The PVA/GO nanocomposites were prepared by an alcoholysis reaction of the above-mentioned PVAc/GO. The 6 wt% NaOH methanol solution was added to 5 wt% PVAc methanol solution with stirring at 42 °C for 2 h to yield PVA. The mole ratio of NaOH to VAc was 0.02. Then the product was extracted for 24 h in a soxhlet extracter using methanol as solvent to remove these impurities. Finally, the product was dried under vacuum at 50 °C for 24 h. The additive amounts of GO were 0 g, 0.01 g, 0.02 g, 0.04 g and 0.08 g, thus the samples were named as PVA, PVA-0.01% GO, PVA-0.02% GO, PVA-0.04% GO and PVA-0.08% GO, respectively.

2.3. Characterizations

2.3.1 Transmission electron microscopy (TEM). TEM was carried out on a Tecnai G^2 F20 microscope with an acceleration voltage of 200 kV to analyse the morphology of GO and nanocomposites. The GO samples were prepared by dropping the diluted GO suspension after being subjected to ultrasonic treatment (480 W) for 30 min on a copper grid and drying in the air at room temperature. The PVA/GO and PVAc/GO nanocomposites were observed as ultrathin sections microtomed using an Ultratome (Leica EM UC6, German) in liquid nitrogen.

2.3.2 Scanning electron microscopy (SEM). Microscopic morphology observations were conducted with a Hitachi S-3400 microscope (Japan) at 5 kV accelerating voltage. The samples of the nanocomposites were fractured in liquid nitrogen and gold-sputtered prior to observation.

2.3.3 X-ray photoelectron spectroscopy (XPS). The XPS of GO was measured on a XSAM800 X-ray photoelectron spectrometer (Kratos) with monochromatic Al Kα as excitation source.

2.3.4 Atomic force microscopy (AFM). AFM micrograph of GO was performed using a Nanoscope Multimode and Explore atomic force microscope (Veeco Instruments, Woodbury, NY). The GO solution of 0.02 mg/mL was dropped onto a freshly cleaved mica surface and dried in a dryer at room temperature before the test. The tapping mode was used and the scan rate was 1.0 Hz.

2.3.5 Fourier-transform infrared (FTIR) spectroscopy. FTIR spectra of the samples were conducted on a Nicolet iS50 FT-IR spectrometer (USA), ranging from 4000 to 400 cm^{-1}. The samples were dried at 50 °C for 12 h in a vacuum oven prior to test.

2.3.6 X-ray diffraction (XRD). XRD patterns were collected on X'Pert Pro X-ray diffractometer using Cu-Ka radiation at an accelerating voltage of 50 kV and a current of 35 mA. The scanning speed was 5°/min and the data were collected at 2θ = 5-50°.

2.3.7 Differential scanning calorimetry (DSC). DSC data were obtained by a NETZCH 204 Phoenix differential scanning calorimeter using nitrogen as the purge gas. The samples of 5-6 mg were first heated from room temperature to 250 °C at a heating rate of 20 °C/min, and held at 250 °C for 5 min to eliminate the prior thermal history and then cooled down to 30 °C at a rate of 10 °C/min, at last heated from 30 °C to 250 °C at a heating rate of 10 °C/min.

2.3.8 Mechanical measurements. The tensile properties of PVA samples were carried out using an INSTRON 5567 (USA) universal testing machine with the crosshead rate of 50 mm/min at room temperature. The reported values were calculated as the averages over five specimens for each group.

2.3.9 Coefficient of moisture permeability (P_{H_2O}). P_{H_2O} of PVA/GO nanocomposite films were measured by a PERME W3/030 moisture permeability testing machine (Jinan Languang, China) according to ISO2556:1974. The samples with the thickness of 150 μm were cut into rounds with the diameter of 5 cm and measured at 100% relative humidity and 25 °C.

3. Results and discussion

3.1. Characterization of GO

The TEM, SEM, AFM images and C1s spectrum of GO

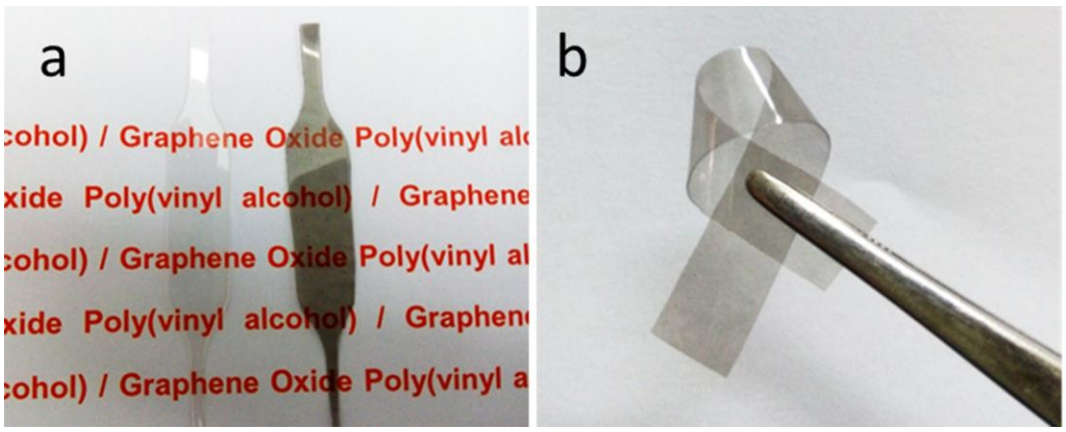

Fig. 3 Digital images of (a) PVA and PVA-0.04 wt% GO nanocomposite film and (b) the crimped sample of PVA-0.04 wt% GO nanocomposite film.

This journal is © The Royal Society of Chemistry 20xx

RSC Advances Accepted Manuscript

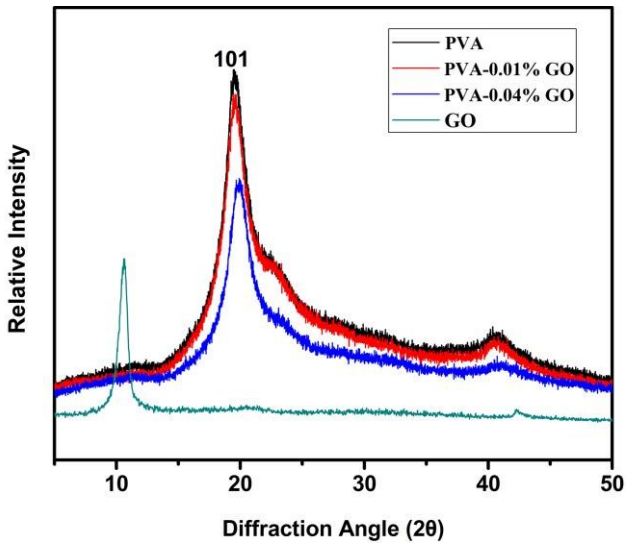

Fig. 4 XRD patterns of GO, pure PVA, and representative PVA/GO nanocomposites.

nanosheets are shown in Fig. 2. It is clearly observed in Fig. 2a that the TEM morphology of the nanosheets with the average size of 1-2 μm is crumpled and partial overlapped. Fig. 2b presents the SEM morphology of the freeze-dried GO. It is a lamellar solid which is easy to be directly intercalated into interlayers by small molecules. As shown in Fig. 2c, the thickness of nanosheets is around 0.8 nm, which clearly indicates the GO is completely exfoliated into single layer.[42] The much higher thickness than that of graphene (0.34 nm) is attributed to the intercalating oxygen-containing functional groups and the absorbed water.[38] XPS is used to investigate the surface chemical composition of GO. Just as shown in Fig. 2d, the C1s XPS spectrum of GO presents a significant extent of oxidization with four types of carbon atoms: C–C (284.6 eV), C–O (C-OH) (286.5 eV), C=O (287.0 eV) and –COO (288.5 eV), which proves that the hydroxyl, epoxide, and carboxyl groups are generated after oxidation.[41] The results above indicate the successful preparation of GO nanosheets from graphite.

3.2. Dispersion of GO in PVA and hydrogen bonding interactions between GO and PVA.

Fig. 3 presents the digital images of PVA and PVA/GO samples. As seen in Fig. 3a, the composite films are shinning, smooth and uniform. The additive GO disperse well in the composite films and no agglomeration of GO can be seen. The words under the PVA-0.04% GO nanocomposite film can be seen clearly, presenting a good transparency of the composite films. The crimped sample of PVA-0.04 % GO nanocomposite film in Fig. 3b demonstrates the high flexibility and toughness of the composite films.

XRD is an important tool for characterizing the delamination and dispersion of GO in the nanocomposites. Fig. 4 illustrates the representative XRD patterns of GO, PVA, and PVA/GO nanocomposites. The featured diffraction peak of GO sheets appears at 2θ = 10.6°, corresponding to the *d*-spacing of 0.83 nm according to Bragg diffraction formula,[43] which is in good accordance with the result of AFM image. The XRD patterns of PVA/GO composite films with different GO loadings show no GO characteristic peak but only the (101) diffraction peak of PVA crystal at 2θ = 19.6°, which may be explained as that the GO sheets are fully intercalated without restacking together and disperse homogeneously in the PVA matrix.[44] Additionally, the intensity of the (101) diffraction peak shows a slight drop with the increasing GO content, inferring that the crystallinity of the nanocomposites has the same trend. This finding will be further proved in the following DSC analysis.

TEM and SEM images are observed to further invest the delamination and dispersion of GO in the nanocomposites. Fig. 5a and 5b show typical TEM images of the ultrathin sections of PVAc/GO and PVA/GO nanocomposites. It can be clearly seen that the additive GO in PVAc/GO and PVA/GO nanocomposites are completely intercalated, uniformly dispersed and highly oriented along the surface of the samples after in situ polymerization. These oriented GO platelets are separated by polymer nanolayers to form a nanobrick wall structure. In addition, the GO in PVAc/GO and PVA/GO nanocomposites shows much crumpled surface texture, which would provide additional interactions and improve the compatibility with the polymer chains. Besides, the TEM morphology of GO observed in PVA-0.04% GO presents more wrinkles and ripples at the edge of GO than that in PVAc/GO, which can be explained as that the strong hydrogen bonding interactions between the oxygen containing functional groups of GO and the hydroxyl groups on the PVA molecular chains cause the tortuosity and distortion of GO.[45] It would allow the nanosheets completely compatible with the PVA chains and play an important role in enhancing the mechanical interlocking and load transfer within the matrix as well as the barrier properties.[4] Fig. 5c and 5d present the SEM morphology of the fracture surface of PVA and typical PVA/GO nanocomposites. The fracture surface of pure PVA is smooth, whereas that of PVA/GO nanocomposites presents a ductile fracture with slight roughness and some parallel textures. The strong interfacial hydrogen bonding between GO nanosheets and PVA matrix induces a brittle-ductile transition. On the other hand, because of the complete compatibility and the full interaction of polymer chains and crumpled GO, the dispersed GO nanosheets are covered by thick PVA layers, the boundary between the PVA matrix and GO is inconspicuous and indistinguishable to be visualized in the SEM image.[46]

Fig. 6 demonstrates the typical digital images of PVAc/GO and PVA/GO nanocomposite solution before and after 2 h of centrifugation at the speed of 15000r/min. The first row is the digital image of the nanocomposite solution before centrifugation while the second row presents that after centrifugation treatment. It's clear that after high-speed centrifugation, most of the GO in PVAc/GO are separated with PVA solution; whereas most of GO in PVA/GO, as the alcoholysis product of PVAc/GO, are still restricted in the polymer solution. The distinct phenomena demonstrate that the interfacial interactions of GO and PVA are surely much

RSC Advances Accepted Manuscript

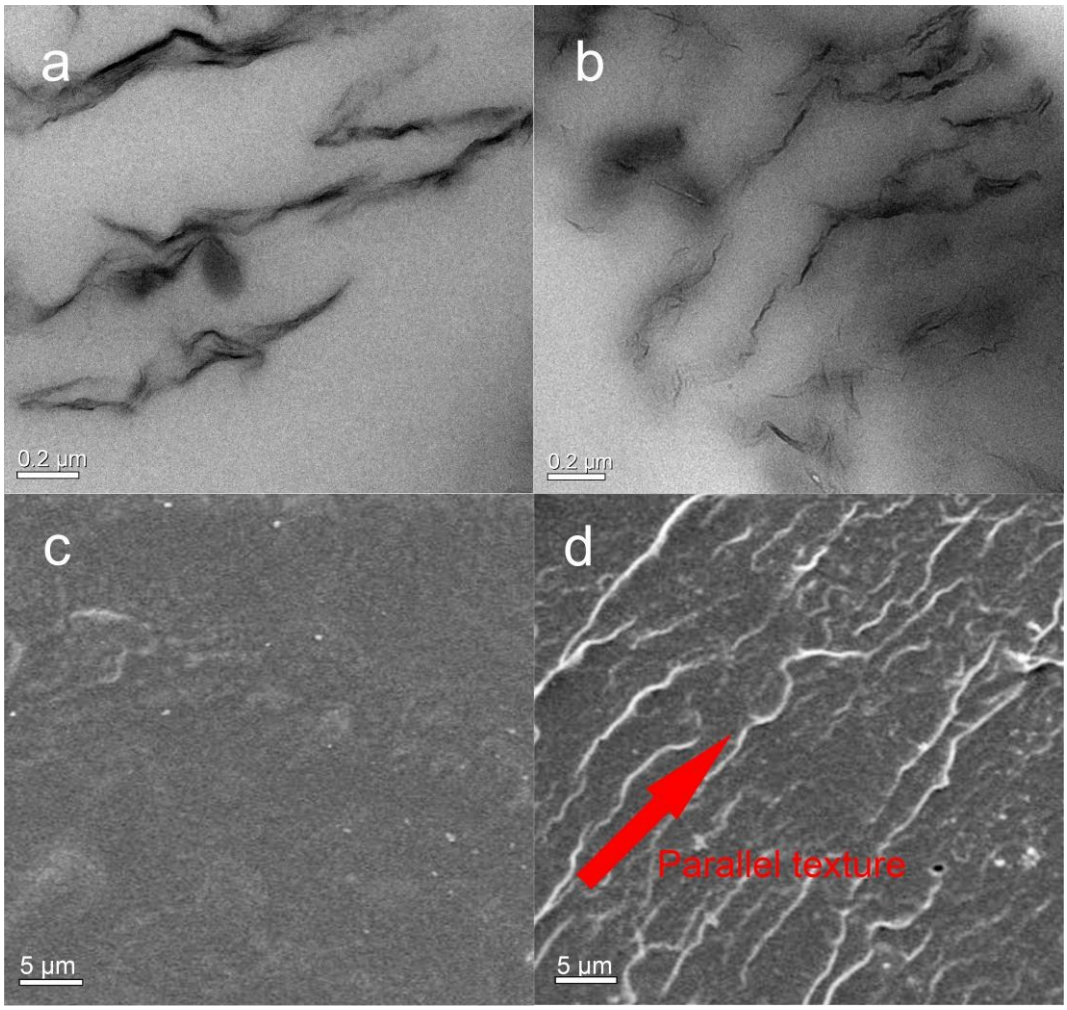

Fig. 5 (a, b) TEM images of the ultrathin sections of PVAc/GO and PVA/GO nanocomposites (with 0.04 wt% GO). (c, d) SEM images of the fracture surfaces of PVA and PVA-0.04 % GO.

stronger than that of GO and PVAc due to the existence of hydrogen bonding interactions.

In order to further observe the hydrogen bonding interactions between the GO and PVA, FTIR tests were carried

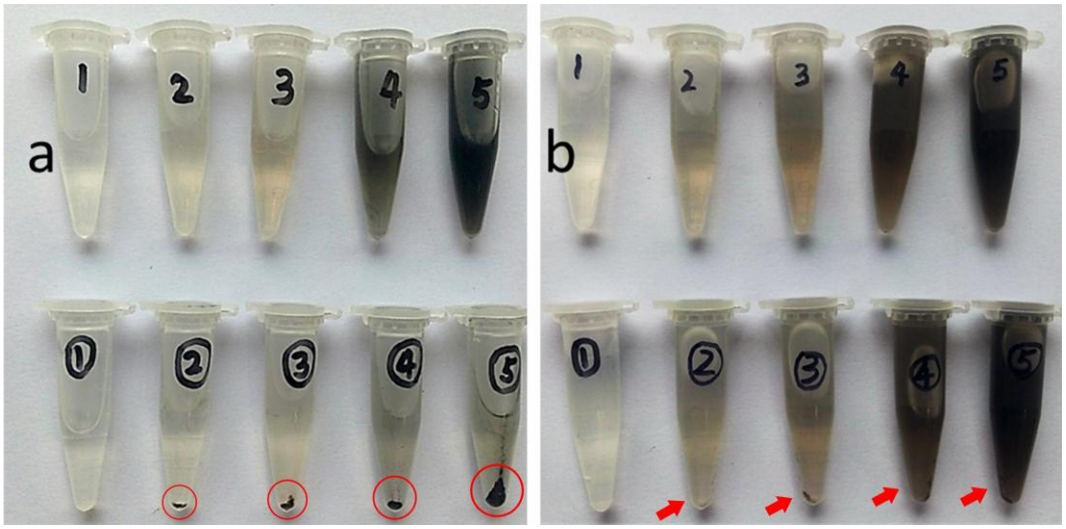

Fig. 6 Digital images of (a) PVAc/GO solution and (b) PVA/GO solution before and after 2 h of high-speed centrifugation.

This journal is © The Royal Society of Chemistry 20xx

RSC Advances Accepted Manuscript

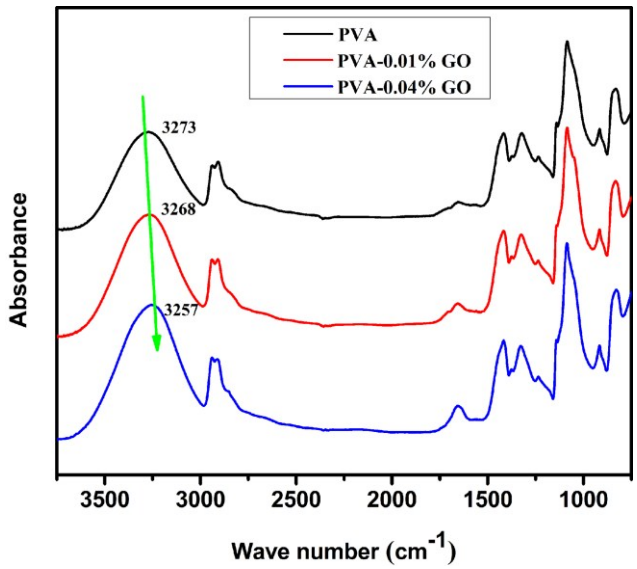

Fig. 7 FTIR spectra of PVA and PVA/GO nanocomposites.

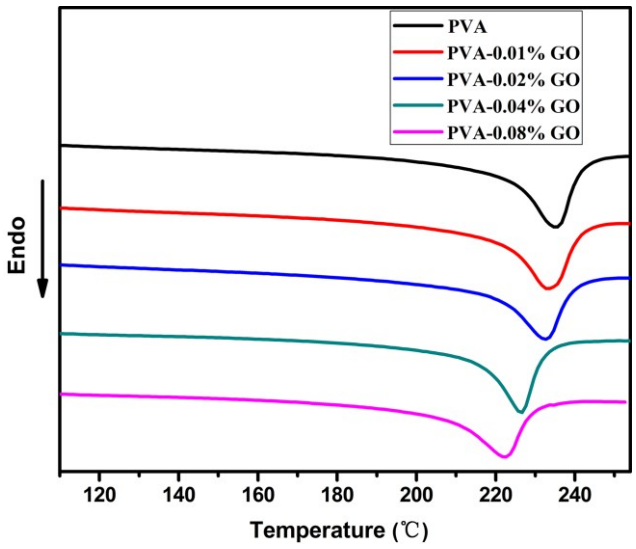

Fig. 8 DSC curves of pure PVA and PVA/GO nanocomposites with various GO loadings.

out. It is well known that the –OH stretching bands is sensitive to the hydrogen bond. As seen in Fig. 7, the FTIR spectra of PVA/GO nanocomposites are highly similar to that of pure PVA, which indicate that the addition of GO has few influence on the structures of PVA. At the same time, it can be clearly seen that the peak for –OH stretching shifts from 3273 cm^{-1} in the pure PVA to the lower wavenumbers of 3268 cm^{-1} in the PVA-0.01% GO and 3257 cm^{-1} in the PVA-0.04% GO, respectively, indicating the decline of the hydrogen bonding among the hydroxyl groups in PVA chains. These results suggest the existence of hydrogen bonding interactions between the oxygen containing functional groups of GO and the hydroxyl groups on the PVA molecular chains is to the detriment of hydrogen bonding among PVA chains.[47]

To understand how the GO could affect the thermal properties of the matrix polymer in the nanocomposites, DSC analysis was performed to observe the melting temperature (T_m) and crystallinity (X_c) of PVA and PVA/GO nanocomposites. The crystallinity of samples was calculated based on the following equation:

$$X_c(\%) = \frac{\Delta H_m}{\Delta H_0} \times 100 \quad (1)$$

where ΔH_m is the measured melting endothermic enthalpy, ΔH_0 is the theoretical melting enthalpy of 100% crystalline PVA, which has a value of 156 J/g.[48] The DSC curves of neat PVA and PVA/GO nanocomposites with various GO loadings are shown in Fig. 8. The details of the thermal properties are also presented in Table 1. The T_m of neat PVA is 235.2 °C, it declines gradually with the increase of GO content and at last reaches to the minimum value of 222.7 °C at the highest GO content of 0.08 wt%. The X_c of the nanocomposites has the same trend and it decreases from 40.0% of pure PVA to 34.0% of PVA-0.08% GO. The most probable reason is that the dispersed intercalated GO particles act as obstacles for the mobility and flexibility of PVA chains to fold and join the crystallinity growth front.[49] The strong hydrogen bonding interactions between the GO and PVA chains would also damage the ordered arrangement of PVA chains, thus decrease the crystallinity of PVA to some extent and result in the decline of T_m.

Table 1 Thermal properties and crystallinity of PVA and PVA/GO nanocomposites.

Samples	T_m (°C)	ΔH_m (J·g^{-1})	Xc (%)
PVA	235.2±5.0	62.3±1.8	40.0±1.3
PVA-0.01% GO	233.3±5.2	61.5±1.5	39.4±1.1
PVA-0.02% GO	232.7±4.0	59.2±1.1	38.0±0.8
PVA-0.04% GO	226.4±4.2	54.9±1.4	35.2±1.0
PVA-0.08% GO	222.7±4.3	52.9±1.5	34.0±1.1

3.3. Mechanical properties of PVA/GO nanocomposites.

The homogeneity of composites and the strong interfacial interactions between the nanosheets and the polymer matrix should have significant effect on the mechanical properties. Fig. 9 shows the mechanical properties of PVA/GO nanocomposites: tensile strength (left) and elongation at break (right) as a function of GO loadings. The details of the mechanical properties are summarized in Table 2. As seen, both the tensile strength and Young's modulus apparently exhibit an enhancing trend with the increasing GO content at low loading level. The tensile strength increases from 42.3 MPa of pure PVA to 50.8 MPa of PVA-0.04% GO and Young's modulus increases from 1477 to 2123 MPa. Such large improvement in the mechanical properties at such low loading of GO can be attributed to a combination of the superior tensile strength (130 GPa) and Young's modulus (0.25 TPa) of GO nanosheets,[50,51] the excellent delamination and uniform dispersion of the GO nanosheets throughout the polymer matrix, the aligned distribution of GO parallel to the surface of the sample films and the strong hydrogen bonding interactions

RSC Advances Accepted Manuscript

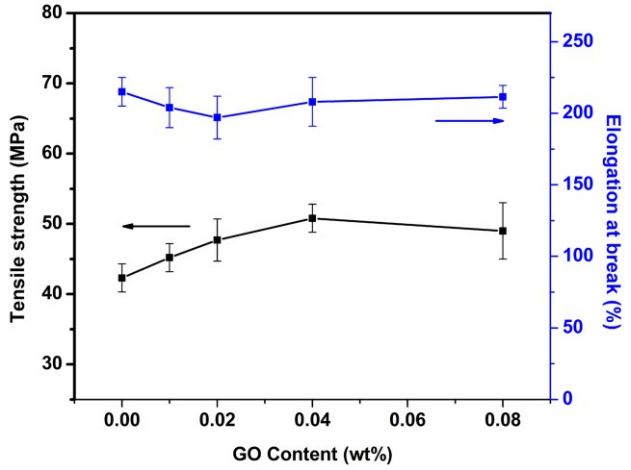

Fig. 9 Mechanical properties of PVA/GO nanocomposites: tensile strength (left axis) and elongation at break (right axis) versus GO loadings.

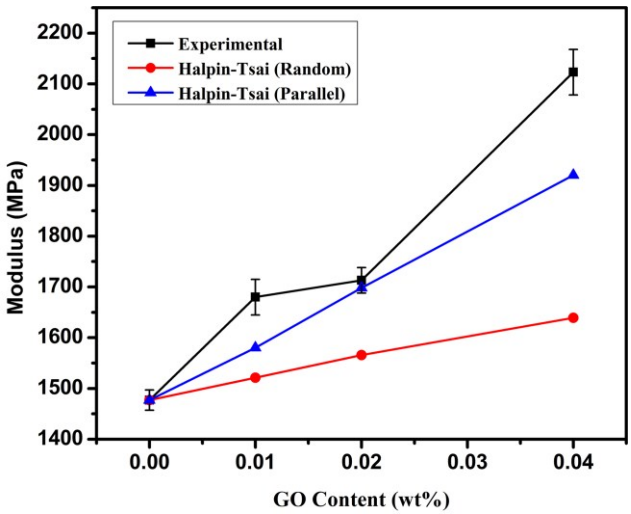

Fig. 10 Experimental Young's moduli of the PVA/GO nanocomposites and those calculated using Halpin–Tsai models with two extreme cases: the random orientation and parallel dispersion of GO nanosheets in the PVA matrix.

Table 2 Mechanical Properties of PVA and PVA/GO nanocomposites.

Samples	Tensile strength (MPa)	Young's modulus (MPa)	Elongation at break (%)
PVA	42.3	1477	215
PVA-0.01% GO	45.2	1680	204
PVA-0.02% GO	47.7	1713	197
PVA-0.04% GO	50.8	2123	208
PVA-0.08% GO	49.0	1954	211.5

between the GO and polymer chains. In addition, the crumpled texture would also provide additional interactions to enhance the mechanical properties. The slight decrease in tensile strength and Young's modulus of PVA-0.08% GO is attributed to the incomplete intercalation, weakening the efficiency of the mechanical improvement. It is worthwhile to mention that the elongation at break is in the range of 197-215%, which can be taken as little change in elongation behaviour and is different from some previous literatures,[22,52] in which the addition of GO or graphene embrittles the PVA matrix and the elongation at break declines markedly. This is because that the strong H-bonding interactions between the GO surface and PVA matrix cause typical restriction in the movement of the polymer chains and decrease the elongation behaviour.[24,52] On the contrary, the decreased crystallinity of the matrix would lower the restriction of PVA polymer chains in nanocomposites and increase the elongation behaviour. The unchanged elongation behaviour is attributed to the exact counterbalance of the decreased elongation behaviour and the improved elongation behaviour. Namely, the incorporation of GO in this system results in not only strong but also tough PVA composites.

The Halpin–Tsai model, which is the most widely used model to simulate the modulus of unidirectional or randomly distributed filler-reinforced composites, [23,46,52] is used here to further analyse the dispersed state of GO in the PVA matrix and its reinforcement effect on mechanical properties. Considering the GO nanosheets are random orientation or parallel distribution to the surface of the nanocomposite films, the Halpin–Tsai model is written as following equations:

$$E_{random} = \left[\frac{3}{8}\left(\frac{(2l/3t)\eta_L V_G}{1-\eta_L V_G}\right) + \frac{5}{8}\left(\frac{1+2\eta_L V_G}{1-\eta_L V_G}\right)\right] E_P \quad (2)$$

$$E_{parallel} = \left[\frac{1+(2l/3t)\eta_L V_G}{1-\eta_L V_G}\right] E_P \quad (3)$$

$$\eta_L = \frac{(E_G/E_P)-1}{(E_G/E_P)+(2l/3t)} \quad (4)$$

$$\eta_T = \frac{(E_G/E_P)-1}{(E_G/E_P)+2} \quad (5)$$

where E_{random} and $E_{parallel}$ represent the Young's moduli of PVA/GO nanocomposites with randomly distributed GO and aligned GO parallel to the sample surface, respectively. E_G and E_P represent the Young's moduli of the GO and PVA matrix. l, t, and V_G refer to the length, thickness, and volume fraction of GO in the composites, respectively. The Young's modulus of the PVA sample is 0.15 GPa according to the experimental results. The Young's modulus of chemically reduced monolayer GO was previously reported as 0.25 TPa,[51] which could be approximately similar to that of the GO nanosheets in the PVA/GO composites used in our study. The thickness and average length of GO nanosheets are 0.8 nm and 1 μm, respectively, as determined by AFM and TEM images. Since we used weight content (wt%) in our work, it needs to be converted to volume content (vol%) using the below equation:

$$v = \frac{w\,\rho_P}{w\,\rho_P+(1-w)\rho_G} \quad (6)$$

where v and w refer to volume content and weight content of GO, ρ_P and ρ_G represent the density of PVA matrix and GO

RSC Advances Accepted Manuscript

This journal is © The Royal Society of Chemistry 20xx

nanosheets, which can be taken as 1.3 g/cm^3 and 2.2 g/cm^3,[24] respectively. As seen Fig. 10, the experimental Young's modulus greatly exceeded the model predictions. As the Halpin–Tsai model was developed for rigid nanofillers with limited interactions between the nanofiller and the polymer, the incomparable reinforcement of Young's modulus in our PVA/GO nanocomposites is not only attributed to the factors mentioned above, but also attributed to the successful and effective load transfer to the crumpled GO nanosheets across the PVA–GO interface due to hydrogen bond.[23,46] It's notable that the experimental data obtained from PVA/GO nanocomposites provide a much closer fit to the theoretical simulation results under the hypothesis that GO is parallel distribution to the surface of the nanocomposite films. This demonstrates that the dispersed GO nanosheets prefer to aligning parallel to the sample surface within the nanocomposites, which are consistent with the TEM and SEM images of the morphology of nanocomposites presented in Fig. 5. The PVA/GO nanocomposites with such unprecedented increase of Young's modulus and high orientation of GO have the potential to produce high modulus and high strength fibers.[53,54]

3.4. Water vapor barrier Properties of PVA/GO nanocomposites.

Because of the abundance of hydroxyl groups, PVA shows high affinity to water, which results in the extremely poor water vapor barrier properties and limited applications. The addition of GO could also enhance the water vapor barrier properties of PVA. Just as seen in Fig. 11, compared with pure PVA films, the water vapor permeability of GO/PVA nanocomposites declines significantly. The P_{H_2O} decreases from 3.0×10^{-12} g·cm/(cm^2·s·Pa) to 0.66×10^{-12} g·cm/(cm^2·s·Pa) by adding only 0.04 wt% GO, corresponding to 78% reduction than that of neat PVA. The dramatic decline in water vapor permeability can be attributed to many factors: (i) the excellent barrier properties of GO nanosheets, (ii) tremendous aspect ratio of GO, (iii) complete delamination and dispersion of GO in the PVA matrix, (iv) aligned distribution of GO parallel to the surface of the sample films and (v) strong interfacial adhesion between the GO nanosheets and the polymer chains.

As the permeability of gas is a kind of diffusion process of single molecule through the polymer matrix, which is generally supposed to be a function of two processes: solubility and diffusion.[55,56] Assuming that the permeation behaviour of water molecules through the films is ideal, the permeability of water follows the solution–diffusion model expressed as below:

$$P = D \times S \quad (7)$$

where P represents the permeability coefficient, D and S represent the diffusion coefficient and solubility coefficient, respectively. Because the polymer crystals and GO are both gas impermeable, the barrier properties of PVA, as a semi-crystalline polymer, are influenced by both the nanoplatelets and crystalline structure.[10] High crystallinity is beneficial to the improvement of gas barrier. But as shown in Fig. 8, the crystallinity shows a slight decrease from 40.0% to 34.0%.

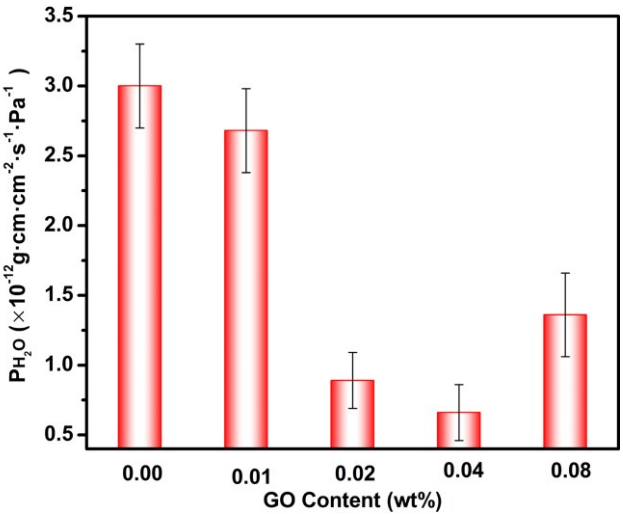

Fig. 11 P_{H_2O} for PVA/GO nanocomposite films versus GO loadings.

Therefore, the remarkable improvement on barrier properties of PVA/GO nanocomposites is mainly attributed to the addition of GO. On the one hand, the additive impermeable GO nanosheets with tremendous aspect ratio are completely delaminated and aligned parallel to the surface of the matrix films, which would lead to the formation of perfect nanobrick wall structure (shown in Fig. 5) and bring in much longer and more tortuous pathway for the permeating molecules, thus causing the significant decline in the diffusion coefficient D.[10,56,57] On the other hand, the crumpled GO nanosheets can interact fully with PVA chains through strong hydrogen bonding, which would thicker and denser the PVA matrix. It will cause the decrease of free volume as well as the available area for diffusion, thereby resulting in the decrease of the solubility coefficient S.[45,51] Both the decrease of D and S would cause the great decline of P_{H_2O}. Such significant decrease of water vapor permeability at such high relative humility will greatly expand the application of PVA in the fields of packaging industry, electronics, fuel cell industry, and etc.

4. Conclusions

In conclusion, the homogeneous PVA/GO nanocomposites have been prepared successfully by one-step in situ polymerization. The GO were completely intercalated, uniformly dispersed and highly oriented along the surface of nanocomposite films. The dispersed and intercalated GO in the nanocomposites had strong hydrogen bond interactions with the PVA matrix. In addition, the mechanical properties had been strikingly enhanced at extremely low loadings of GO (only 0.01-0.08 wt%) due to the effective load transfer between the PVA matrix and GO via strong hydrogen bonding interactions. At the same time, the water vapor barrier properties of PVA/GO nanocomposites had also been significantly improved due to the formation of perfect nanobrick wall structure. This in situ method opened a novel strategy to produce PVA/GO or PVA/graphene nanocomposites. It not only realized the

RSC Advances Accepted Manuscript

delamination and dispersion of GO, but also improved the mechanical properties and water vapor barrier properties of PVA by one step. Besides, the enhanced mechanical properties and water vapor barrier properties would greatly expand the application of PVA in fiber, packaging, electronics, fuel cell industry, and so on.

Acknowledgements

This work was supported by the Research Center for Application of Graphene (Sichuan University-WuXi) and the State Key Laboratory of Polymer Materials Engineering (Grant no. sklpme2014-3-06).

Notes and references

1 N. Tenn, N. Follain, K. Fatyeyeva, J. M. Valleton, F. P. Epaillard, N. Delpouve and S. Marais, *J. Phys. Chem. C.*, 2012, **116**, 12599.
2 J. Gaume, P. W. Chung, A. Rivaton, S. Thérias and J.-L. Gardette, *RSC Adv.*, 2011, **1**, 1471.
3 T. Pan, S. Xu, Y. Dou, X. Liu, Z. Li, J. Han, H. Yan and M. Wei, *J. Mater. Chem. A.*, 2015, **3**, 12350.
4 Y.-H. Yang, L. Bolling, M. A. Priolo and J. C. Grunlan, *Adv. Mater.*, 2013, **25**, 503.
5 S. Mollá and V. Compañ, *J. Power Sources*, 2011, **196**, 2699.
6 S. Tripathi, G. K. Mehrotra, P. K. Dutta, *Carbohyd. Polym.*, 2010, **79**, 711.
7 C. C. DeMerlis and D. R. Schoneker, *Food Chem. Toxicol.*, 2003, **41**, 319.
8 X.-Q. Hu, D.-Z. Ye, J.-B. Tang, L.-J. Zhang and X. Zhang, *RSC Adv.*, 2016, **6**, 13797.
9 B. Zhang, S. Xu, H. Tang and P. Wu, *RSC Adv.*, 2013, **3**, 8372.
10 H. M. Kim, J. K. Lee and H. S. Lee, *Thin Solid Films*, 2011, **519**, 7766.
11 J. Wang, W. Qiu, N. Wang and L. Li, *RSC Adv.*, 2015, **5**, 84578.
12 Y. Cui, S. Kumar, B. R. Konac and D. V. Houckec, *RSC Adv.*, 2015, **5**, 63669.
13 K. S. Novoselov, A. K. Geim, S. V. Morozov, D. Jiang, Y. Zhang, S. V. Dubonos, I. V. Grigorieva and A. A. Firsov, *Science*, 2004, **306**, 666.
14 N. A. Kotov, *Nature*, 2006, **442**, 254.
15 D. Chen, H. Zhang, Y. Liu and J. Li, *Energy Environ. Sci.*, 2013, **6**, 1362.
16 W. K. Chee, H. N. Lim, N. M. Huang and I. Harrison, *RSC Adv.*, 2015, **5**, 68014.
17 P. Bhawal, S. Ganguly, T. K. Chaki and N. C. Das, *RSC Adv.*, 2016, **6**, 20781.
18 J. Wang, X. Wang, C. Xu, M. Zhang and X. Shang, *Polym Int.*, 2011, **60**, 816.
19 N. B. Milosavljević, L. M. Kljajević, I. G. Popović, J. M. Filipović and M. T. K. Krušić, *Polym Int.*, 2010, **59**, 686.
20 J. Zhang, P. Hu, X. Wang, Z. Wang, D. Liu, B. Yang and W. Cao, *J. Mater. Chem.*, 2012, **22**, 18283.
21 N. A. Zubair, N. A. Rahman, H. N. Lim, R. M. Zawawi and Y. Sulaiman, *RSC Adv.*, 2016, **6**, 17720.
22 J. Li, L. Shao, X. Zhou and Y. Wang, *RSC Adv.*, 2014, **4**, 43612.
23 Y. Xu, W. Hong, H. Bai, C. Li, G. Shi, *Carbon*, 2009, **47**, 3538.
24 J. Liang, Y. Huang, L. Zhang, Y. Wang, Y. Ma, T. Guo and Y. Chen, *Adv. Funct. Mater.*, 2009, **19**, 2297.
25 H. K. F. Cheng, N. G. Sahoo, Y. P. Tan, Y. Pan, H. Bao, L. Li, S. H. Chan and J. Zhao. *ACS Appl. Mater. Interfaces*, 2012, **4**, 2387.
26 M. Cano, U. Khan, T. Sainsbury, A. O'Neill, Z. Wang, I. T. McGovern, W. K. Maser, A. M. Benito, J. N. Coleman, *Carbons*, 2013, **52**, 363.
27 X. Zhao, Q. Zhang, Y. Hao, Y. Li, Y. Fang and D. Chen, *Macromolecules*, 2010, **43**, 9411.
28 Y. Guo, C. Bao, L. Song, B. Yuan and Y. Hu, *Ind. Eng. Chem. Res.*, 2011, **50**, 7772.
29 X. Wang, Y. Hu, L. Song, H. Yang, W. Xing and H. Lu, *J. Mater. Chem.*, 2011, **21**, 4222.
30 Y. Huang, Y. Qin, Y. Zhou, H. Niu, Z.-Z. Yu and J.-Y. Dong, *Chem. Mater*., 2010, **22**, 4096.
31 Z. Xu and C. Gao, *Macromolecules*, 2010, **43**, 6716.
32 C. C. DeMerlis and D. R. Schoneker, *Food Chem. Toxicol.*, 2003, **41**, 319.
33 L. Jiang, T. Yang, L. Peng and Y. Dan, *RSC Adv.*, 2015, **5**, 86598.
34 P. Liu, K. Gong, P. Xiao and M. Xiao, *J. Mater. Chem.*, 2000, **10**, 933.
35 S. Stankovich, D. A. Dikin, G. H. B. Dommett, K. M. Kohlhaas, E. J. Zimney, E. A. Stach, R. D. Piner, S. T. Nguyen, R. S. Ruoff, *Nature*, 2006, **442**, 282.
36 A. Lucas, C. Zakri, M. Maugey, M. Pasquali, P. Schoot and P. Poulin, *J. Phys. Chem.* C, 2009, **113**, 20599.
37 J. H. Bang and K. S. Suslick, *Adv. Mater.*, 2010, **22**, 1039.
38 G.-Q. Qi, J. Cao, R.-Y. Bao, Z.-Y. Liu, W. Yang, B.-H. Xie and M.-B. Yang, *J. Mater. Chem. A*, 2013, **1**, 3163.
39 E. R. F. Sarabia, J. A. G. Juárez, G. R. Corral, L. E. Segura and I. G. Gómez, *Ultrasonics*, 2000, **38**, 642.
40 W. S. Hummers Jr and R. E. Offeman, *J. Am. Chem. Soc.*, 1958, **80**, 1339.
41 Y. Li, Y. Xu, T. Zhou, A. Zhang and J. Bao, *RSC Adv.*, 2015, **5**, 32469.
42 M. Hirata, T. Gotou, S. Horiuchi, M. Fujiwara and M. Ohba, *Carbon*, 2004, **42**, 2929.
43 W. M. Itano, J. J. Bollinger, J. N. Tan, B. Jelenković, X.-P. Huang and D. J. Wineland, *Science*, 1998, **279**, 686.
44 J. Li, L. Shao, L. Yuan and Y. Wang, *Mater. Des.*, 2014, **54**, 520.
45 M. A. Rafiee, J. Rafiee, Z. Wang, H. Song, Z.-Z. Yu and N. Koratkar, *ACS Nano,* 2009, **3**, 3884.
46 S. Roy, X. Tang, T. Das, L. Zhang, Y. Li, S. Ting, X Hu and C. Y. Yue, *ACS Appl. Mater. Interfaces*, 2015, **7**, 3142.
47 X. Yang, L. Li, S. Shang and X. Tao, *Polymer*, 2010, **51**, 3431.
48 L. Wei and Y. Lin, *J. Appl. Polym. Sci.*, 2013, **129**, 3757.
49 S. S. Ray and M. Bousmina, *Macromol. Chem. Phys.,* 2006, **207**, 1207.
50 C. Lee, X. Wei, J. W. Kysar and J. Hone, *Science*, 2008, **321**, 385.
51 C. G. Navarro, M. Burghard and K. Kern, *Nano Lett.*, 2008, **8**, 2045.
52 X. Zhao, Q. Zhang and D. Chen, *Macromolecules,* 2010, **43**, 2357.
53 J. Li, L. Shao, X. Zhou and Y. Wang, *RSC Adv.*, 2014, **4**, 43612.
54 P. Zhang, T. Zhou, L. He, S. Zhang, J. Sun, J. Wang, C. Qin and L. Dai, *RSC Adv.*, 2015, **5**, 55492.
55 H.-D. Huang, P.-G. Ren, J. Chen, W.-Q. Zhang, X. Ji and Z.-M. Li, *J. Membr. Sci.*, 2012, **409**, 156.
56 E. L. Cussler, S. E. Hughes, W. J. Ward and R. Aris, *J. Membr. Sci.*, 1988, **38**, 161.
57 H. W. Kim, H. W. Yoon, S.-M. Yoon, B. M. Yoo, B. K. Ahn, Y. H. Cho, H. J. Shin, H. Yang, U. Paik, S. Kwon, J.-Y. Choi and H. B. Park, *Science*, 2013, **342**, 91.

RSC Advances Accepted Manuscript

This journal is © The Royal Society of Chemistry 20xx

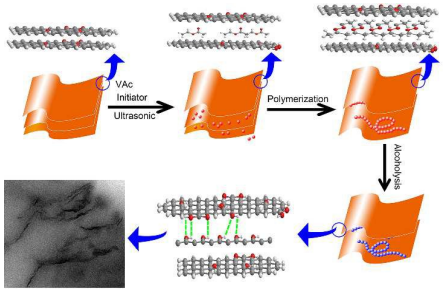

The novelty of the work: A novel and one-step in situ polymerization method for preparing the poly(vinyl alcohol) (PVA)/graphene oxide (GO) nanocomposites.

RSC Advances Accepted Manuscript